
One-Step Offline Distillation of Diffusion-based Models via Koopman Modeling

Nimrod Berman*
Ben-Gurion University of the Negev

Ilan Naiman*
Ben-Gurion University of the Negev

Moshe Eliasof
University of Cambridge

Hedi Zisling
Ben-Gurion University of the Negev

Omri Azencot
Ben-Gurion University of the Negev

Abstract

Diffusion-based generative models have demonstrated exceptional performance, yet their iterative sampling procedures remain computationally expensive. A prominent strategy to mitigate this cost is *distillation*, with *offline distillation* offering particular advantages in terms of efficiency, modularity, and flexibility. In this work, we identify two key observations that motivate a principled distillation framework: (1) while diffusion models have been viewed through the lens of dynamical systems theory, powerful and underexplored tools can be further leveraged; and (2) diffusion models inherently impose structured, semantically coherent trajectories in latent space. Building on these observations, we introduce the *Koopman Distillation Model (KDM)*, a novel offline distillation approach grounded in Koopman theory—a classical framework for representing nonlinear dynamics linearly in a transformed space. KDM encodes noisy inputs into an embedded space where a learned linear operator propagates them forward, followed by a decoder that reconstructs clean samples. This enables single-step generation while preserving semantic fidelity. We provide theoretical justification for our approach: (1) under mild assumptions, the learned diffusion dynamics admit a finite-dimensional Koopman representation; and (2) proximity in the Koopman latent space correlates with semantic similarity in the generated outputs, allowing for effective trajectory alignment. Empirically, KDM achieves state-of-the-art performance across standard *offline distillation* benchmarks—improving FID scores by up to 40% in a single generation step. All implementation details and code for the experimental setups are provided in our **GitHub** - <https://github.com/azencot-group/KDM>, or in our **project page** - <https://sites.google.com/view/koopman-distillation-model>.

1 Introduction

Diffusion-based generative models [62], including score-based and flow-matching variants [24, 41], have become ubiquitous across a wide range of domains—from images and videos to audio and time series [14, 25, 35, 12]. These models now surpass approaches such as GANs and VAEs in terms of sample quality, while also exhibiting greater training stability. Despite these advantages, one of their key limitations remains the high computational cost associated with sampling [53, 58, 45]. Generating a single high-fidelity sample typically requires executing a lengthy iterative process, progressively refining random noise through dozens or even hundreds of model evaluations [24].

*Equal contribution

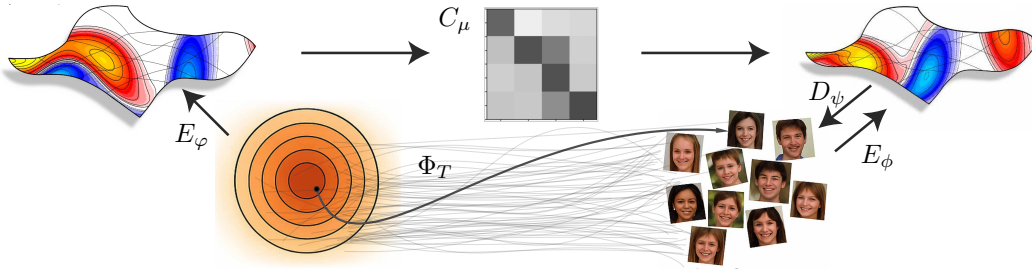


Figure 1: A Gaussian sample (bottom left) evolves into a clean image (bottom right) via nonlinear dynamics Φ_T . Leveraging the Koopman framework, learned encoders E_φ and E_ψ transform noise and image into an embedding space where the evolution becomes linear under C_μ (top).

A widely adopted strategy to address this involves minimizing the number of inference steps [63], for example by leveraging improved numerical solvers or designing more expressive noise schedules, enabling high-quality generation with significantly fewer iterations. Another increasingly popular alternative is *distillation* [58], where a student model learns to emulate the behavior of a teacher model. Distillation approaches vary in supervision and setup: in online distillation, the student directly learns from the teacher’s predictions during training, with the teacher providing trajectory information across time steps. In contrast, *offline distillation* relies on precomputed noise-image pairs generated by the teacher, and the student learns without further querying the teacher model. Offline distillation offers key advantages over online approaches: by training on precomputed noise-image pairs, it avoids the need for multi-stage training, it reduces the amount of neural function evaluations required by the teacher model, it allows to filter privacy-violating synthetic data generated by the teacher before distillation, and it eliminates the overhead of keeping the teacher model in memory throughout training [17, 19]. This leads to more private, scalable training and allows for broader reuse of distilled data across different student architectures and settings.

Towards developing a principled distillation method, we identify two key observations that guide our approach: (1) While denoising-based methods leverage dynamical systems perspectives for both general generative modeling [66, 41] and distillation [78, 9], a wide range of powerful tools from dynamical systems theory remain underexplored; (2) Trained diffusion models impose a structured organization on the latent space, coherently mapping noisy inputs toward clean data. Specifically, our empirical analysis suggests that semantically related images tend to originate from nearby points in the noise space.

Building on these observations, we propose leveraging a dynamical systems approach that has not yet been explored in the context of distillation: Koopman operator theory. This theory is a classical yet recently revitalized approach for representing nonlinear systems with linear dynamics in an embedded space [36, 57]. The core idea is that by mapping the system into a suitable embedding space, its evolution becomes linear. Thus, learning the diffusion process then reduces to jointly learning these embeddings and the linear operator. While Koopman operators are typically infinite-dimensional, we prove that an exact finite-dimensional representation exists under mild assumptions [26]. Moreover, prior work suggests that the Koopman operator preserves the structure inherent to certain dynamical systems [22, 6]. This motivates the use of Koopman theory to harness the observed coherent semantic structure in diffusion dynamics, offering a principled foundation for accurate teacher model distillation. To this end, we formally connect the observed structure in diffusion models to the Koopman framework by proving that this structure is preserved within the learned dynamical representation.

In practice, we propose KDM (*Koopman Distillation Model*), a framework for modeling diffusion processes through linear evolution in a learned embedding space. Given a noisy input, an encoder maps it into an embedding space where a learned Koopman operator evolves it forward, and a decoder reconstructs the clean sample. A schematic illustration of our framework is presented in Fig. 1. The training objective encourages semantic preservation (via reconstruction loss), accurate latent linear dynamics (via Koopman consistency), and fidelity in output space (via prediction and adversarial losses). This design naturally yields fast, single-step generation, while preserving structural coherence distillation. We evaluate our method on the offline distillation benchmark, while

adding two higher-resolution datasets, and achieve state-of-the-art results in both unconditional and conditional generation. Compared to prior offline work, our approach improves FID by up to 40% while requiring only a single generation step. These results demonstrate the effectiveness of our Koopman-based formulation in bridging the performance gap with online methods, offering a fast and high-fidelity offline diffusion model distillation. **Our key contributions are:**

1. *Observing diffusion dynamics.* We identify, analyze and formalize two key observations: (i) tools from dynamical systems theory, specifically Koopman operator theory, remain underexplored in diffusion modeling and distillation. (ii) training induces coherent semantic organization in noise space. These insights motivate a structure-promoting dynamics-aware approach to distillation.
2. *A principled and practical Koopman-based distillation framework.* We develop a theoretical foundation proving the existence of finite-dimensional Koopman representations and semantic structure preservation under mild assumptions and introduce a simple, scalable encoder–linear-dynamics–decoder architecture that preserves the teacher generation dynamics semantic structure.
3. *State-of-the-art results.* We conduct a comprehensive unconditional and conditional evaluation showing that our method consistently outperforms prior offline distillation approaches, achieving up to 40% FID improvement—while enabling efficient, single-step generation.

2 Related Work

Generative Modeling. Deep generative models have made significant progress in recent years, with diffusion models emerging as a leading framework for high-quality image, audio, and molecular generation. Building on principles from nonequilibrium thermodynamics and score matching [62, 66], these models define a forward process that gradually corrupts data with noise and learn to reverse it via a neural network-based denoising process. Variants like DDPMs [24] and score-based generative models [66] have shown competitive performance across a wide range of benchmarks, often surpassing VAEs and GANs [34, 21] in sample fidelity and diversity.

Accelerating Diffusion Sampling. Diffusion models generate high-quality samples but are slow due to iterative sampling. One approach improves integration using higher-order solvers and expressive noise schedules [63, 43], achieving high-quality results in significantly fewer steps. Another class of approaches seeks to distill a student model from a pre-trained teacher, reducing the sampling process to a single or few steps. Online distillation techniques [44, 58] supervise the student directly with teacher predictions during training, but require continuous access to the full teacher model, resulting in high memory and compute overhead. Recent methods demonstrate high-quality one-step generation across CIFAR-10, ImageNet, and text-to-image benchmarks [75, 81], using objectives based on distribution matching [75], score identity [81], adversarial training [59, 61], and consistency models [65, 32] among others [9, 46, 52, 82]. Offline distillation methods [19] rely on teacher-generated noise-data pairs and decouple student training from the teacher, enabling more scalable and modular pipelines. As far as we know, current distillation methods largely unexplored Koopman-based perspectives and their relation to the teacher’s underlying dynamics.

Koopman-Based Modeling. Koopman operator theory provides a powerful framework for modeling nonlinear dynamical systems via linear operators acting on observable functions [36, 57]. This view has been applied to tasks such as deep learning of dynamical systems [69, 47, 73, 55], sequential disentanglement [4], and control [23]. A related strand of work focuses on identifying coherent sets—regions of the state space that evolve coherently over time—using Koopman-based embeddings [50, 18]. While these works exploit the Koopman structure for interpretability or stability, our work is, to our knowledge, the first to use Koopman-based modeling for distilling diffusion models. In this context, we demonstrate that the learned embedding space in diffusion models encodes semantically meaningful structure, and we leverage this to design a principled offline distillation framework.

3 Mathematical Background

Deterministic Diffusion Sampling. We consider deterministic sampling in diffusion models, as introduced in the EDM framework [28]. A pre-trained diffusion model defines a time-indexed denoising vector field $f_\theta : \mathbb{R}^n \times [0, T] \rightarrow \mathbb{R}^n$, which maps a noisy latent state $x_t \in \mathbb{R}^n$ at time $t \in [0, T]$ toward the data manifold (at time 0). Sampling is performed by solving the reverse-time ordinary differential equation (ODE),

$$\frac{d x_t}{d t} = f_\theta(x_t, t), \quad x_T \sim \mathcal{N}(0, \sigma_T^2 \mathbf{I}), \quad (1)$$

integrated backward from a Gaussian sample x_T at time T to a clean sample x_0 at time $t = 0$. The function f_θ is typically trained to approximate the score function $\nabla_{x_t} \log p_t(x_t)$ or a reparameterization thereof, such as the probability flow [66]. These deterministic formulations enable sampling via high-order ODE solvers and provide a tractable setting for distillation and trajectory analysis [28].

Koopman Operator Theory. Let $\Phi_t : \mathbb{R}^n \rightarrow \mathbb{R}^n$ define a (possibly time-dependent) dynamical system mapping states forward in time, i.e., $x_t = \Phi_t(x_0)$. The Koopman operator \mathcal{K}_t [36] is a linear operator that acts on scalar-valued *observables* $g : \mathbb{R}^n \rightarrow \mathbb{C}$ via composition,

$$\mathcal{K}_t g := g \circ \Phi_t, \quad (2)$$

mapping each observable to its pullback along the dynamics. While the original system Φ_t may be nonlinear, \mathcal{K}_t is linear on the space of observables $L^2(\mathbb{C}^n)$ (with respect to a suitable measure) [16]. In classical Koopman theory, this operator is infinite-dimensional. However, if there exists a finite-dimensional subspace $\mathcal{O} = \text{span}\{g_1, \dots, g_d\} \subset L^2(\mathbb{C}^n)$ that is invariant under \mathcal{K}_t for all $t \in [0, T]$, then the dynamics of Φ_t can be exactly represented in this lifted space via a family of linear operators $C_t \in \mathbb{R}^{d \times d}$, $t \in [0, T]$, such that for all $g \in \mathcal{O}$, $\mathcal{K}_t g = C_t g$. This allows modeling nonlinear dynamics through linear evolution in a learned observable space, a principle that underpins our Koopman-based distillation framework.

4 Koopman Distillation of Diffusion Models

We propose *KDM*, a principled offline distillation framework for diffusion models based on Koopman operator theory. The key idea is to model the dynamics of the generative process, specifically the transformation from a noisy sample x_T to its clean counterpart x_0 , as a single-step *linear* evolution in a learned embedding space. This approach enables fast and structure-preserving generation in a single forward pass, without requiring access to the full diffusion trajectory or teacher model at training time.

Dynamical System Perspective on Diffusion Models. We build upon two key observations regarding diffusion models. *First*, diffusion can be understood as a dynamical system, where the evolution of a noisy data point x_t is governed by a time-dependent velocity field, see Eq. (1). This continuous-time formulation admits an integrated flow map Φ_t such that $x_t = \Phi_t(x_0)$, where Φ_t evolves the initial condition x_0 forward in time. This formulation makes it natural to propose adopting a Koopman operator perspective, a novel approach in the context of distillation, which enables the lifting of nonlinear dynamics into a linear evolution in function space under suitable choices of observables, see Eq. (2).

The *second* observation considers the structure of the trained diffusion dynamics. Score-based diffusion models learn the score $\nabla_{x_t} \log p_t(x_t)$ of noise-corrupted data at multiple noise levels and then reverse that specific corruption process using Langevin dynamics [66] or learned reverse kernels [24] to transform Gaussian noise into images. This framework has been unified through the lens of stochastic differential equations (SDEs) by [66]. Flow matching models [41] learn a continuous velocity field that transports a simple reference distribution directly into the data distribution, where sampling is typically performed by integrating the learned ordinary differential equation (ODE). In what follows, we study the structure of the dynamical mapping arising from diffusion-based learning.

We pose the following question: *Is there semantic structure in the generative process of diffusion models?* In general, prior to training, there is no assurance of semantic structure between the noise and data distributions (see Fig. 2, left). However, after training, we observe the emergence of a coherent and semantically meaningful mapping from the Gaussian noise distribution to the data distribution (see Fig. 2, right). Specifically, by utilizing a simple 2D checkerboard toy dataset, we train an EDM [28] model and generate 50,000 samples, recording both the initial noise vectors and their corresponding generated outputs on the checkerboard. We then color-code each sample by its target checker cell and assign the same color to its originating noise vector. This visualization reveals that samples originating from the same semantic region in data space tend to cluster together in noise space, indicating structured and coherent dynamics. Notably, we observe a similar pattern in both flow matching model and our KDM. This emergence of coherent structure, together with prior evidence that the Koopman operator preserves structure in certain dynamical systems [22, 6], highlights the relevance of Koopman theory to diffusion dynamics. Indeed, our theoretical analysis (Sec. 5) establishes a formal link between this observed structure and Koopman theory, motivating its adoption as a principled framework for modeling these dynamics.

Koopman-based Distillation. Our Koopman distillation framework is designed by the following principle: given pairs of noisy and clean data (x_T, x_0) , where $x_0 = \Phi_T(x_T)$ for some unknown

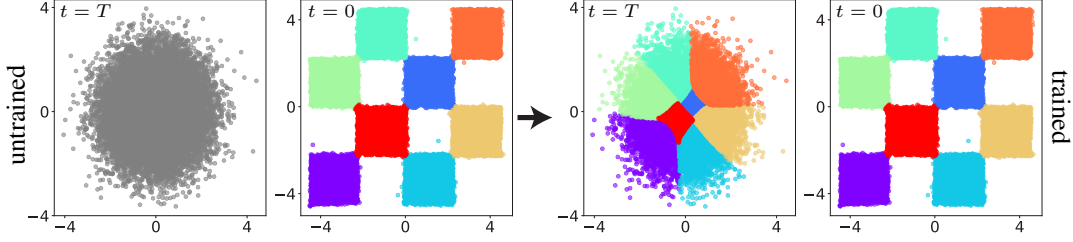


Figure 2: Untrained noise distributions are semantically unstructured (left). Training EDM on the data reveals the emergence of coherent clusters in noise space, i.e., at time T (right).

nonlinear map Φ_t , we seek to model this transformation using a finite-dimensional linear operator in an embedding space, following Koopman theory. To achieve this, we introduce observable functions $\{g_1, g_2, \dots, g_d\}$, parameterized as *encoder networks* E_ϕ, E_φ for x_0, x_T , respectively, that map states from the original data space into a latent observable space. In this space, we assume the dynamics can be modeled linearly by a finite-dimensional Koopman operator linear layer, C_η . Finally, a corresponding *decoder network* D_ψ maps the evolved observables back to the data space. The overall modeling objective becomes:

$$x_0 \approx D_\psi(C_\eta E_\varphi(x_T)) . \quad (3)$$

This formulation distills the potentially complex, nonlinear generative process into a simple one-step linear map in the embedded observables space, while maintaining fidelity to the original dynamics.

Koopman’s Loss Functions. In what follows, $d(\cdot, \cdot)$ denotes a suitable distance function, such as mean squared error (MSE) or a perceptual loss (e.g., LPIPS [77]). To effectively learn the components E_ϕ, D_ψ , and C_η , we define a composite loss comprising three terms (see similar objectives in [47, 3]):

$$\mathcal{L}_{\text{Koopman}} = \mathcal{L}_{\text{rec}} + \mathcal{L}_{\text{lat}} + \mathcal{L}_{\text{pred}} . \quad (4)$$

The first term, the *reconstruction loss* \mathcal{L}_{rec} , ensures that the encoder-decoder pair (E_ϕ, D_ψ) can faithfully reconstruct x_0 :

$$\mathcal{L}_{\text{rec}} = d(x_0, D_\psi(E_\phi(x_0))) . \quad (5)$$

This term regularizes the embedding by encouraging E_ϕ to preserve sufficient semantic information about the data, while not encoding any dynamic features. The second term, the *latent dynamics loss* \mathcal{L}_{lat} , enforces consistency of the linear evolution in the observable space:

$$\mathcal{L}_{\text{lat}} = d(E_\phi(x_0), C_\eta E_\varphi(x_T)) , \quad (6)$$

where C_η is the Koopman operator in latent space. This term ensures that applying C_η to the embedded noisy state $E_\varphi(x_T)$ approximates the embedded clean state $E_\phi(x_0)$. C_η is either implemented with a regular learning linear layer or by a new approach we develop that factorizes the matrix, which enables eigenspectrum control (KDM-F). We describe the decomposition and its merits in App. C.

Finally, the *prediction loss* $\mathcal{L}_{\text{pred}}$ evaluates the full end-to-end prediction after encoding, applying the Koopman operator, and decoding:

$$\mathcal{L}_{\text{pred}} = d(x_0, D_\psi(C_\eta E_\varphi(x_T))) , \quad (7)$$

encouraging the system to accurately predict x_0 from x_T in a single forward pass through the Koopman pipeline. Together, these terms provide complementary supervision signals.

Adversarial Loss. Adversarial frameworks are widely employed in distillation methods [60, 32, 67, 68]. For example, [32] leverages an adversarial loss to enhance the fidelity of one-step generation. Motivated by these approaches, we introduce an auxiliary adversarial loss to further refine the distillation process. Specifically, we introduce a discriminator network D_γ , parameterized by γ , and define the adversarial loss as:

$$\mathcal{L}_{\text{adv}}(\phi, \psi, \gamma) = \mathbb{E}_{x_0 \sim p_{\text{data}}} [\log D_\gamma(x_0)] + \mathbb{E}_{x_T \sim p_{\text{data}}} [\log(1 - D_\gamma(\hat{x}_0))] , \quad (8)$$

where $\hat{x}_0 = D_\psi(C_\eta E_\varphi(x_T))$ is the Koopman-predicted sample. Thus, the final training objective is:

$$\mathcal{L} = \mathcal{L}_{\text{Koopman}} + \lambda_{\text{adv}} \mathcal{L}_{\text{adv}} , \quad (9)$$

where λ_{adv} balances the adversarial component. In practice, throughout our experiments, we choose $\lambda_{\text{adv}} = 0.01$. Importantly, we utilized a simple D_γ with four convolutional layers. By enhancing the perceptual quality of the predictions without altering the fundamental Koopman modeling, this adversarial augmentation strengthens the overall generation performance while preserving the structured distillation at the heart of our method [5]. We present losses and more ablation studies in App. D.1. Additionally, A pseudo-code of our KDM is provided in App. E.1.

Control Modeling for Conditional Dynamics. A crucial aspect of generative modeling with denoising models is the ability to condition generation on auxiliary signals or labels [14]. Koopman theory provides a natural framework to incorporate such conditioning through control signals that influence the Koopman operator [8]. Formally, let c denote the control signal or conditioning variable (e.g., a class label) that we want the generative process to be conditioned on. Our goal is to model the conditional dynamics $\Phi(x_T, c)$. In the Koopman framework, we extend the observable and evolution operators to incorporate c , and formulate the generation as:

$$D_\psi(C_\eta E_\phi(x_T, c) + C_\mu(c), c) \approx \Phi(x_T, c),$$

where $C_\mu(c)$ is a control-dependent modulation term (e.g., a linear transformation of c). This formulation enables our model to adapt its generative trajectory based on the conditioning signal, seamlessly integrating the conditioning mechanism into the Koopman dynamics. We apply this control modeling in our conditional generation experiments.

5 Theoretical Properties of KDM

We now state the **first** key theoretical result, establishing the existence of an exact finite-dimensional Koopman representation under mild conditions. Specifically, for an analytic dynamical system, it is possible to approximate its nonlinear evolution to arbitrary accuracy by a finite-dimensional linear operator acting on lifted coordinates. In particular, a small number of polynomial observables can capture the system’s dynamics with controllable approximation error. This result is significant because it means we can faithfully replicate the complex behavior of the teacher model using a simpler, linear system in a transformed space. In practical terms, it ensures our student can learn to follow the teacher’s dynamics with high accuracy.

Theorem 5.1 (Finite Koopman Operator for Analytic Dynamics). *Let $\Phi : \mathbb{R}^n \rightarrow \mathbb{R}^n$ be an analytic map, and let $x_T \sim \mathcal{N}(0, I_n)$. Then, for any $\epsilon > 0$, there exists a linear operator $C \in \mathbb{R}^{d \times d}$ such that*

$$\mathbb{E} [\|\xi(\Phi(x_T)) - C\xi(x_T)\|^2] \leq \epsilon, \quad (10)$$

where $\xi : \mathbb{R}^n \rightarrow \mathbb{R}^d$ denotes the observable lifting map. Moreover, the required dimension d grows at most polynomially with $1/\epsilon$, and the mapping Φ can be approximated arbitrarily well using multivariate polynomials up to degree d .

The proof builds on the analytic formulation of Φ , allowing a convergent multivariate Taylor expansion [71], and on exact finite-dimensional Koopman operators for polynomial dynamics [26], see App. A.

Our **second** theoretical result concerns the structure induced by the reverse diffusion dynamics, under a set of assumptions established by Thm. 5.1. Under these conditions, the theorem states that proximity in the Koopman coordinate representation at the initial noise time implies semantic similarity between the corresponding samples at data time. In practice, the theorem says that if two inputs start out close together in the transformed space, the images they generate will be semantically similar. This provides a theoretical foundation for the structure-preserving behavior of our model, as observed empirically in Sec. 6.1.

Theorem 5.2 (Semantic Proximity via Koopman-Invariant Coordinates). *Let $\Phi_t : \mathbb{R}^n \rightarrow \mathbb{R}^n$ be the reverse diffusion flow of a trained model (from time T to 0), and let $\mathcal{O} \subset L^2(\mathbb{R}^n)$ be a finite-dimensional subspace such that:*

1. $\mathcal{K}_t \mathcal{O} \subset \mathcal{O}$ for all $t \in [0, T]$,
2. $\exists C_t : \mathbb{R}^d \rightarrow \mathbb{R}^d$ such that $\mathcal{K}_t \xi = \xi \circ \Phi_t = C_t \xi$ for all $\xi \in \mathcal{O}$,
3. Φ_T is locally Lipschitz.

For any $x_T^1, x_T^2 \in \mathbb{R}^n$, define $x_0^j := \Phi_T(x_T^j)$ for $j = 1, 2$, and let $\xi : \mathbb{R}^n \rightarrow \mathbb{R}^d$ be the vector-valued observable $\xi(x) := (\xi_1(x), \dots, \xi_d(x)) \in \mathcal{O}$. Then:

$$\|x_0^1 - x_0^2\| \leq L \cdot \|\Phi_T(x_T^1) - \Phi_T(x_T^2)\| \leq L \cdot \|C_T\| \cdot \|\xi(x_T^1) - \xi(x_T^2)\|.$$

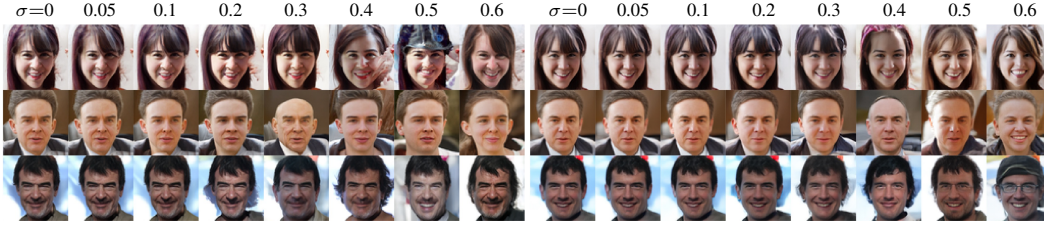


Figure 3: Visualization of vicinity comparison across different noise levels σ . Left: EDM [28]. Right: our method. Each image corresponds to a small perturbation around the original noise sample.

The proof builds on the observation that diffusion model dynamics tend to preserve semantic similarity between inputs and outputs. By leveraging the Koopman operator’s spectral properties, we construct a finite-dimensional space of functions that remains stable under the model’s evolution. Within this space, the Koopman coordinates ξ provide a locally bi-Lipschitz representation, while the reverse diffusion map Φ_T is Lipschitz continuous. Together, these properties ensure that semantically similar inputs remain close throughout the diffusion process. Note that the theorem holds also for $\xi := \text{id}$, i.e., the identity map [48, 15]. The full proof is given in App. B.

6 Experiments

We begin by broadening the investigation of the emergent structure in the dynamics that map noise to images, and its presence in KDM (Sec. 6.1). We then extensively evaluate our method on the offline distillation benchmark (Sec. 6.2), including analyses of computational complexity, data and parameter scaling, and denoiser-agnostic applicability. Additionally, an ablation study of the loss functions is provided in App. D.1. We also provide a code repository of KDM in the supplementary materials.

Setup and evaluation. We follow the protocol of GET [19] for generating noisy-clean pairs and for evaluation, using the CIFAR-10 [37], FFHQ 64×64 [30], and AFHQv2 64×64 [11] datasets. Our training setup matches that of PD [58] and GET [19]. For evaluation, we report image quality using Fréchet Inception Distance (FID) and Inception Score (IS), computed over 50k samples. Both encoders E_φ and E_ϕ , as well as the decoder D_ψ , are implemented as compact UNets with reduced output channels to ensure similar parameters size to the other single-step methods. The discriminator consists of four simple Conv2D layers. Full implementation details are provided in App. E.3.

6.1 Observations of Emergent Latent Structure

Real-world data dynamics: local structure analysis. Extending the 2D toy experiment from Sec. 4, we now explore the high-dimensional FFHQ 64×64 dataset. Since dimensionality reduction can obscure fine-grained patterns, we instead analyze the local neighborhood of a single latent sample $x_T \sim \mathcal{N}(0, I_n)$. We generate perturbed versions $\hat{x}_T = x_T + \varepsilon \cdot \sigma$ with $\varepsilon \sim \mathcal{N}(0, I_n)$, and normalize each \hat{x}_T using its own mean and standard deviation. This setup tests whether semantic structure emerges locally around x_T . We vary $\sigma \in \{0, 0.05, \dots, 0.60\}$ and visualize the outputs in Fig. 3 (left). For all $\sigma < 0.3$, the images remain semantically aligned with the original image (when $\sigma = 0$), indicating local smoothness and manifold adherence. As σ grows, semantics diverge but retain global coherence even at $\sigma = 0.60$. The same experiment on KDM (Fig. 3, right) reveals similar behavior, affirming that KDM preserves the local semantic structure of the original EDM. Our results show that both models organize latent space into meaningful neighborhoods, even in high-dimensional settings.

Visual analysis of dynamics distillation. Beyond preserving local structure, KDM also approximately reproduces the noise-to-image mapping of EDM. When starting from the same noise vector $x_T \sim \mathcal{N}(0, I_n)$, sampled using seeds not seen during training, both EDM (with 79 NFEs) and KDM (with a single NFE) generate perceptually similar outputs (see Fig. 4). This suggests that KDM generalizes well beyond its training data and effectively distills the mapping from noise to data. We observe this consistency across multiple datasets and include further qualitative results in App. D.2. To quantify this, we generate 50k samples using both methods and compare outputs using LPIPS and MSE. KDM achieves scores of 0.13 (LPIPS) and 0.009 (MSE), in contrast to 0.48 and 0.57 when comparing randomly permuted images, demonstrating the similarity between the models’ generation. To complement quantitative metrics, we conduct a human study where participants choose the more realistic image collage between our model and EDM (Fig. 4; details in App. E.4). Evaluators showed no clear preference: 55% of 300 choices favored our model, highlighting its strong fidelity.

Outliers and their relation to the dynamics structure. We analyze a recurring failure mode in both the teacher and distilled models: the generation of outlier samples that fall outside the designated



Figure 4: Sampled images using 79 NFEs with EDM [28] (left), and using 1 NFE with KDM (right).

checkerboard regions. These out-of-distribution points often appear in the final outputs and reflect a limitation in capturing the intended data distribution. To investigate their origin, we trace these outliers back through the generation process and identify two primary sources: (1) the tails of the Gaussian prior and (2) regions near decision boundaries between adjacent checkerboard cells. Fig. 5(c) shows this behavior for the distilled model (black crosses denote outliers); additional comparisons with the teacher are provided in App. E.6. These findings suggest that the model’s dynamics are more error-prone in high-uncertainty regions, offering potential directions for improvement. Integrating more robust sampling techniques or leveraging self-supervised signals may help mitigate such failures. This insight could also inform future efforts in uncertainty estimation.

6.2 One-step Generation Results

Unconditional and Conditional Generation with CIFAR-10. We evaluate our method on the standard offline distillation benchmark introduced in [19], which tests the ability to distill a pre-trained EDM on the CIFAR-10 dataset. While EDM generates samples in 35 NFEs, our approach achieves the results in a single NFE. Tab. 1 reports unconditional generation results, where our method achieves state-of-the-art (SOTA) performance, surpassing the previous offline baseline in both FID and IS. In particular, we observe $\approx 25\%$ reduction in FID over the best prior method. Tab. 3 shows results for class-conditional generation, where our model yields $\approx 40\%$ improvement in FID and superior IS. Although offline distillation offers advantages in efficiency, privacy, and flexible deployment [17, 19], a performance gap with online methods remains. This may partly be because online approaches leverage the full generation trajectory, whereas, in the offline pairwise setup, methods only observe two endpoints, placing them at a natural disadvantage. Our results demonstrate a substantial step toward closing this gap. Furthermore, unlike prior methods that rely on architectural assumptions [20, 39], our approach is denoiser-agnostic and successfully distills both EDM and flow matching (FM) models (see Tab. 1), demonstrating broad applicability. Finally, we implemented a factorized KDM (KDM-F). Since every matrix C_η is diagonalizable up to an arbitrarily small perturbation of the entries [2], we can write: $C_\eta = PAP^{-1}$ where $P \in \mathbb{C}^{d \times d}$ is an invertible matrix and $\Lambda = \text{diag}(\lambda_1, \dots, \lambda_d) \in \mathbb{C}^{d \times d}$. While enabling efficient implementation of spectral penalties on Λ (see complexity analysis below), this approach preserves strong performance and accuracy.

Unconditional Generation with FFHQ and AFHQv2. To assess the scalability of KDM to higher-resolution data, we evaluate our method on FFHQ and AFHQv2, distilling each into a single-step generator and assessing performance both quantitatively (Tab. 3) and qualitatively (App. D.2). Our method yields FID scores approximately $2.5\times$ higher than EDM, similar to the degradation observed on CIFAR-10. Due to the high computational cost, we omit GET results: training a single model takes 5–7 weeks on an A6000 GPU, which is technically infeasible in our computational resources. We also exclude ImageNet, as large-scale training with EDM [28] is computationally infeasible for us.

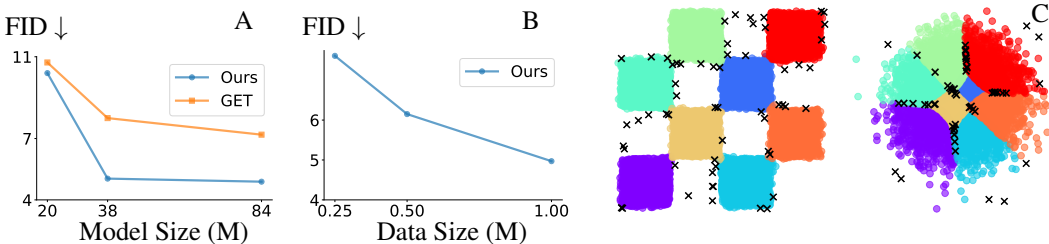


Figure 5: A) Model size vs FID. B) Data Size vs FID. C) Outlier analysis

Table 1: Generative performance on unconditional CIFAR-10.

Models (\downarrow) / Metrics (\rightarrow)	NFE \downarrow	FID \downarrow	IS \uparrow
Diffusion Models			
DDPM [24]	1000	3.17	9.46
Score SDE [63]	2000	2.2	9.89
EDM [30]	35	2.04	9.84
Continuous Flows			
Flow Matching (Diffusion) [40]	183	8.06	-
Flow Matching (OT) [70]	50	4.94	-
2-rf++ [39]	1	3.07	-
GANs			
StyleGAN2 [31]	1	8.32	9.18
StyleGAN-XL [29]	1	1.85	-
Diffusion Distillation			
KD [44]	1	9.36	8.36
PD [58]	1	9.12	-
DFNO [79]	1	4.12	-
iCD-EDM (LPIPS) [64]	1	2.83	9.54
CTM (LPIPS) [64]	1	1.98	-
ECM [20]	1	4.54	-
Offline Distillation			
GET [19]	1	6.91	9.16
KDM(EDM)	1	4.97	9.22
KDM(FM)	1	5.91	8.86
KDM-F(EDM)	1	4.68	9.08

Table 2: Generative performance on class-conditional CIFAR-10.

Models (\downarrow) / Metrics (\rightarrow)	NFE \downarrow	FID \downarrow	IS \uparrow
GANs			
BigGAN [7]	1	14.73	9.22
StyleGAN2-ADA [29]	1	2.42	10.14
Diffusion Distillation			
Guided Dist. ($w = 0.3$) [49]	1	7.34	8.90
ECM [20]	1	3.81	-
Offline Distillation			
GET [19]	1	6.25	9.40
KDM(EDM)	1	3.56	9.54
KDM-F(EDM)	1	3.24	9.68

Table 3: Generative performance on unconditional generation on FFHQ 64×64 and AFHQv2 64×64 . *Indicates our reproduction.

Models (\downarrow) / Metrics (\rightarrow)	NFE \downarrow	FID \downarrow	IS \uparrow
FFHQ 64×64			
EDM*	79	2.47	3.37
KDM(EDM)	1	6.54	3.12
AFHQv2 64×64			
EDM*	79	2.02	9.04
KDM(EDM)	1	4.85	8.25

Scalability in Parameters and Data. Offline distillation inherently supports architectural independence from the teacher model, allowing flexible scaling of the student to meet diverse deployment needs [19, 20]. To assess this, we evaluate our method against GET across three model sizes—20M, 38M, and 84M parameters (Fig. 5A). Our method consistently outperforms GET in FID scores at all scales, with especially notable gains at higher capacities (e.g., 4.89 vs. 7.19 at 84M), demonstrating its effectiveness for both lightweight and high-capacity settings. In parallel, we investigate how performance scales with training data size, a key factor in offline distillation. Following GET [19], we train on 250K, 500K, and 1M samples and report FID scores on unconditional CIFAR-10 in Fig. 5B. Results show that more data yields better generation quality. For instance, increasing the dataset from 250K to 1M samples results in a $\approx 33\%$ FID reduction, showing the importance of data scale. While our method remains data-efficient, additional data can enhance performance.

Complexity Analysis. Offline distillation can offer advantages over online methods, both memory-wise and time-wise [19]. KDM further improves over GET. As shown in Tab. 4, it matches GET in parameter count but achieves a $4\times$ speedup per training iteration and over $8\times$ faster sampling. Notably, KDM-F (App. C) maintains this efficiency even with spectral regularization. These results underscore the practical scalability of our approach.

Table 4: Parameters in millions, time in seconds. RTX 4090 GPU used with batch size 128.

Metric	GET	KDM	KDM + EL	KDM-F + EL
Params(M)	62	62	62	65
Train (s)	3.60	0.91	4.82	0.97
Sampling (s)	937	114	114	116

7 Discussion

In this work, we present two key observations. First, we reinterpret the distillation process through the lens of dynamical systems theory. Second, we uncover the semantical structure in the mapping from latent space to data space in trained diffusion dynamics. Motivated by these insights, we propose a Koopman-based framework for distilling diffusion models, bridging operator theory and generative

modeling. We theoretically establish the existence of a Koopman operator that captures the underlying generative process, and demonstrate, both theoretically and empirically, that our method preserves its structure. This perspective also offers insights into potential failure modes. Beyond its conceptual contributions, our approach is practical and efficient, achieving state-of-the-art single-step offline distillation. We further analyze its robustness and scalability. We hope this work lays the foundation for future directions, including leveraging richer training signals and extending distillation techniques to advanced text-to-image generative models. See App. F for further discussion.

Acknowledgments

This research was partially supported by an ISF grant 668/21, an ISF equipment grant, and by the Israeli Council for Higher Education (CHE) via the Data Science Research Center, Ben-Gurion University of the Negev, Israel.

References

- [1] M. S. Albergo, M. Goldstein, N. M. Boffi, R. Ranganath, and E. Vanden-Eijnden. Stochastic interpolants with data-dependent couplings. *arXiv preprint arXiv:2310.03725*, 2023.
- [2] S. Axler. *Linear algebra done right*. Springer, 2015.
- [3] O. Azencot, N. B. Erichson, V. Lin, and M. Mahoney. Forecasting sequential data using consistent koopman autoencoders. In *International Conference on Machine Learning*, pages 475–485. PMLR, 2020.
- [4] N. Berman, I. Naiman, and O. Azencot. Multifactor sequential disentanglement via structured koopman autoencoders. In *The Eleventh International Conference on Learning Representations, ICLR*, 2023.
- [5] Y. Blau and T. Michaeli. The perception-distortion tradeoff. In *Proceedings of the IEEE conference on computer vision and pattern recognition*, pages 6228–6237, 2018.
- [6] N. Boullé and M. J. Colbrook. Multiplicative dynamic mode decomposition. *arXiv preprint arXiv:2405.05334*, 2024.
- [7] A. Brock, J. Donahue, and K. Simonyan. Large scale gan training for high fidelity natural image synthesis. *arXiv preprint arXiv:1809.11096*, 2018.
- [8] S. L. Brunton and J. N. Kutz. *Modern Koopman Theory for Dynamical Systems*. SIAM, 2022.
- [9] D. Chen, Z. Zhou, J.-P. Mei, C. Shen, C. Chen, and C. Wang. A geometric perspective on diffusion models. *arXiv preprint arXiv:2305.19947*, 2023.
- [10] Y. Chen and U. Vaidya. Sample complexity for nonlinear dynamics. *arXiv preprint arXiv:1810.11747*, 2018.
- [11] Y. Choi, Y. Uh, J. Yoo, and J.-W. Ha. Stargan v2: Diverse image synthesis for multiple domains. In *Proceedings of the IEEE/CVF conference on computer vision and pattern recognition*, pages 8188–8197, 2020.
- [12] A. Coletta, S. Gopalakrishnan, D. Borrajo, and S. Vyetenko. On the constrained time-series generation problem. *Advances in Neural Information Processing Systems*, 36:61048–61059, 2023.
- [13] V. De Bortoli, J. Thornton, J. Heng, and A. Doucet. Diffusion schrödinger bridge with applications to score-based generative modeling. *Advances in Neural Information Processing Systems*, 34:17695–17709, 2021.
- [14] P. Dhariwal and A. Nichol. Diffusion models beat gans on image synthesis. *Advances in neural information processing systems*, 34:8780–8794, 2021.
- [15] A. S. Dogra and W. Redman. Optimizing neural networks via koopman operator theory. *Advances in Neural Information Processing Systems*, 33:2087–2097, 2020.
- [16] T. Eisner, B. Farkas, M. Haase, and R. Nagel. *Operator theoretic aspects of ergodic theory*, volume 272. Springer, 2015.
- [17] V. Fernandez, P. Sanchez, W. H. L. Pinaya, G. Jacenków, S. A. Tsafaris, and J. Cardoso. Privacy distillation: reducing re-identification risk of multimodal diffusion models. *arXiv preprint arXiv:2306.01322*, 2023.

- [18] G. Froyland, S. Lloyd, and A. Quas. Coherent structures and isolated spectrum for perron–frobenius cocycles. *Ergodic Theory and Dynamical Systems*, 30(3):729–756, 2010.
- [19] Z. Geng, A. Pokle, and J. Z. Kolter. One-step diffusion distillation via deep equilibrium models. *Advances in Neural Information Processing Systems*, 36:41914–41931, 2023.
- [20] Z. Geng, A. Pokle, W. Luo, J. Lin, and J. Z. Kolter. Consistency models made easy. *arXiv preprint arXiv:2406.14548*, 2024.
- [21] I. Goodfellow, J. Pouget-Abadie, M. Mirza, B. Xu, D. Warde-Farley, S. Ozair, A. Courville, and Y. Bengio. Generative adversarial nets. In *Advances in Neural Information Processing Systems*, pages 2672–2680, 2014.
- [22] P. Goyal, S. Yıldız, and P. Benner. Deep learning for structure-preserving universal stable koopman-inspired embeddings for nonlinear canonical hamiltonian dynamics. *Machine Learning: Science and Technology*, 6(1):015063, 2025.
- [23] M. Han, J. Euler-Rolle, and R. K. Katzschmann. Desko: Stability-assured robust control with a deep stochastic koopman operator. In *International conference on learning representations (ICLR)*, 2022.
- [24] J. Ho, A. Jain, and P. Abbeel. Denoising diffusion probabilistic models. In *Advances in Neural Information Processing Systems*, volume 33, pages 6840–6851, 2020.
- [25] J. Ho, T. Salimans, A. Gritsenko, W. Chan, M. Norouzi, and D. J. Fleet. Video diffusion models. *Advances in Neural Information Processing Systems*, 35:8633–8646, 2022.
- [26] L. C. Jacob, M. Schoukens, and R. Tóth. Finite dimensional koopman form of polynomial nonlinear systems. *IFAC-PapersOnLine*, 56(2):6423–6428, 2023.
- [27] S. Jayasumana, S. Ramalingam, A. Veit, D. Glasner, A. Chakrabarti, and S. Kumar. Rethinking fid: Towards a better evaluation metric for image generation. *arXiv preprint arXiv:2401.09603*, 2024.
- [28] T. Karras, M. Aittala, T. Aila, and S. Laine. Elucidating the design space of diffusion-based generative models. *Advances in neural information processing systems*, 35:26565–26577, 2022.
- [29] T. Karras, M. Aittala, J. Hellsten, S. Laine, J. Lehtinen, and T. Aila. Training generative adversarial networks with limited data. *Advances in neural information processing systems*, 33:12104–12114, 2020.
- [30] T. Karras, S. Laine, and T. Aila. A style-based generator architecture for generative adversarial networks. In *Proceedings of the IEEE/CVF conference on computer vision and pattern recognition*, pages 4401–4410, 2019.
- [31] T. Karras, S. Laine, M. Aittala, J. Hellsten, J. Lehtinen, and T. Aila. Analyzing and improving the image quality of stylegan. In *Proceedings of the IEEE/CVF conference on computer vision and pattern recognition*, pages 8110–8119, 2020.
- [32] D. Kim, C. Lai, W. Liao, N. Murata, Y. Takida, T. Uesaka, Y. He, Y. Mitsufuji, and S. Ermon. Consistency trajectory models: Learning probability flow ODE trajectory of diffusion. In *The Twelfth International Conference on Learning Representations, ICLR. OpenReview.net*, 2024.
- [33] D. P. Kingma and J. Ba. Adam: A method for stochastic optimization. In Y. Bengio and Y. LeCun, editors, *3rd International Conference on Learning Representations, ICLR 2015, San Diego, CA, USA, May 7-9, 2015, Conference Track Proceedings*, 2015.
- [34] D. P. Kingma and M. Welling. Auto-encoding variational bayes. In *International Conference on Learning Representations (ICLR)*, 2014.
- [35] Z. Kong, W. Ping, J. Huang, K. Zhao, and B. Catanzaro. Diffwave: A versatile diffusion model for audio synthesis. *arXiv preprint arXiv:2009.09761*, 2020.
- [36] B. O. Koopman. Hamiltonian systems and transformation in hilbert space. *Proceedings of the National Academy of Sciences*, 17(5):315–318, 1931.
- [37] A. Krizhevsky, G. Hinton, et al. Learning multiple layers of features from tiny images. Technical report, Toronto, ON, Canada, 2009.
- [38] T. Kynkäänniemi, T. Karras, M. Aittala, T. Aila, and J. Lehtinen. The role of imagenet classes in fréchet inception distance. *arXiv preprint arXiv:2203.06026*, 2022.

- [39] S. Lee, Z. Lin, and G. Fanti. Improving the training of rectified flows. *Advances in Neural Information Processing Systems*, 37:63082–63109, 2024.
- [40] Y. Lipman, R. T. Chen, H. Ben-Hamu, M. Nickel, and M. Le. Flow matching for generative modeling. *arXiv preprint arXiv:2210.02747*, 2022.
- [41] Y. Lipman, E. Hajiramezanali, M. Mahdavi, A. Benson, A. Vahdat, S. Koyejo, and D. Yang. Flow matching for generative modeling. In *International Conference on Machine Learning (ICML)*, 2023.
- [42] A. Lozano-Durán and G. Arranz. Information-theoretic formulation of dynamical systems: causality, modeling, and control. *Physical Review Research*, 4(2):023195, 2022.
- [43] C. Lu, Y. Zhou, F. Bao, J. Chen, C. Li, and J. Zhu. Dpm-solver: A fast ode solver for diffusion probabilistic model sampling in around 10 steps. *Advances in Neural Information Processing Systems*, 35:5775–5787, 2022.
- [44] E. Luhman and T. Luhman. Knowledge distillation in iterative generative models for improved sampling speed. *arXiv preprint arXiv:2101.02388*, 2021.
- [45] S. Luo, Y. Tan, L. Huang, J. Li, and H. Zhao. Latent consistency models: Synthesizing high-resolution images with few-step inference. *arXiv preprint arXiv:2310.04378*, 2023.
- [46] W. Luo, T. Hu, S. Zhang, J. Sun, Z. Li, and Z. Zhang. Diff-instruct: A universal approach for transferring knowledge from pre-trained diffusion models. *Advances in Neural Information Processing Systems*, 36:76525–76546, 2023.
- [47] B. Lusch, J. N. Kutz, and S. L. Brunton. Deep learning for universal linear embeddings of nonlinear dynamics. *Nature communications*, 9(1):4950, 2018.
- [48] A. Mauroy, Y. Susuki, and I. Mezić. Introduction to the Koopman operator in dynamical systems and control theory. *The koopman operator in systems and control: concepts, methodologies, and applications*, pages 3–33, 2020.
- [49] C. Meng, R. Rombach, R. Gao, D. Kingma, S. Ermon, J. Ho, and T. Salimans. On distillation of guided diffusion models. In *Proceedings of the IEEE/CVF Conference on Computer Vision and Pattern Recognition*, pages 14297–14306, 2023.
- [50] I. Mezić. Spectral properties of dynamical systems, model reduction and decompositions. *Nonlinear Dynamics*, 41:309–325, 2005.
- [51] D. Muthirayan and P. P. Khargonekar. Online learning robust control of nonlinear dynamical systems. *arXiv preprint arXiv:2106.04092*, 2021.
- [52] T. H. Nguyen and A. Tran. Swiftbrush: One-step text-to-image diffusion model with variational score distillation. In *Proceedings of the IEEE/CVF Conference on Computer Vision and Pattern Recognition*, pages 7807–7816, 2024.
- [53] A. Q. Nichol and P. Dhariwal. Improved denoising diffusion probabilistic models. In *International conference on machine learning*, pages 8162–8171. PMLR, 2021.
- [54] M. Otani, R. Togashi, Y. Sawai, R. Ishigami, Y. Nakashima, E. Rahtu, J. Heikkilä, and S. Satoh. Toward verifiable and reproducible human evaluation for text-to-image generation. In *Proceedings of the IEEE/CVF Conference on Computer Vision and Pattern Recognition*, pages 12345–12354, 2023.
- [55] S. E. Otto and C. W. Rowley. Linearly recurrent autoencoder networks for learning dynamics. *SIAM Journal on Applied Dynamical Systems*, 18(1):558–593, 2019.
- [56] F. Philipp, M. Schaller, K. Worthmann, S. Peitz, and F. Nueske. Error bounds for kernel-based approximations of the koopman operator. *arXiv preprint arXiv:2301.08637*, 2023.
- [57] C. W. Rowley, I. Mezić, S. Bagheri, P. Schlatter, and D. S. Henningson. Spectral analysis of nonlinear flows. *Journal of fluid mechanics*, 641:115–127, 2009.
- [58] T. Salimans and J. Ho. Progressive distillation for fast sampling of diffusion models. *arXiv preprint arXiv:2202.00512*, 2022.
- [59] A. Sauer, F. Boesel, T. Dockhorn, A. Blattmann, P. Esser, and R. Rombach. Fast high-resolution image synthesis with latent adversarial diffusion distillation. In *SIGGRAPH Asia 2024 Conference Papers*, pages 1–11, 2024.

- [60] A. Sauer, D. Lorenz, A. Blattmann, and R. Rombach. Adversarial diffusion distillation. *arXiv preprint arXiv:2311.17042*, 2023.
- [61] A. Sauer, D. Lorenz, A. Blattmann, and R. Rombach. Adversarial diffusion distillation. In *European Conference on Computer Vision*, pages 87–103. Springer, 2024.
- [62] J. Sohl-Dickstein, E. Weiss, N. Maheswaranathan, and S. Ganguli. Deep unsupervised learning using nonequilibrium thermodynamics. In *International conference on machine learning*, pages 2256–2265. pmlr, 2015.
- [63] J. Song, C. Meng, and S. Ermon. Denoising diffusion implicit models. *arXiv preprint arXiv:2010.02502*, 2020.
- [64] Y. Song and P. Dhariwal. Improved techniques for training consistency models. *arXiv preprint arXiv:2310.14189*, 2023.
- [65] Y. Song, P. Dhariwal, M. Chen, and I. Sutskever. Consistency models. In *International Conference on Machine Learning, ICML*, volume 202 of *Proceedings of Machine Learning Research*, pages 32211–32252. PMLR, 2023.
- [66] Y. Song, J. Sohl-Dickstein, D. P. Kingma, A. Kumar, S. Ermon, and B. Poole. Score-based generative modeling through stochastic differential equations. In *International Conference on Learning Representations (ICLR)*, 2021.
- [67] A. N. Specified. Fast high-resolution image synthesis with latent adversarial diffusion distillation. *arXiv preprint arXiv:2403.12015*, 2024.
- [68] A. N. Specified. Sdxl-lightning: Progressive adversarial diffusion distillation. *arXiv preprint arXiv:2402.13929*, 2024.
- [69] N. Takeishi, Y. Kawahara, and T. Yairi. Learning koopman invariant subspaces for dynamic mode decomposition. *Advances in neural information processing systems*, 30, 2017.
- [70] A. Tong, K. Fatras, N. Malkin, G. Huguët, Y. Zhang, J. Rector-Brooks, G. Wolf, and Y. Bengio. Improving and generalizing flow-based generative models with minibatch optimal transport. *arXiv preprint arXiv:2302.00482*, 2023.
- [71] L. N. Trefethen. *Approximation theory and approximation practice, extended edition*. SIAM, 2019.
- [72] R. Vershynin. *High-dimensional probability: An introduction with applications in data science*, volume 47. Cambridge university press, 2018.
- [73] E. Yeung, S. Kundu, and N. Hodas. Learning deep neural network representations for koopman operators of nonlinear dynamical systems. In *2019 American Control Conference (ACC)*, pages 4832–4839. IEEE, 2019.
- [74] T. Yin, M. Gharbi, T. Park, R. Zhang, E. Shechtman, F. Durand, and B. Freeman. Improved distribution matching distillation for fast image synthesis. *Advances in neural information processing systems*, 37:47455–47487, 2024.
- [75] T. Yin, M. Gharbi, R. Zhang, E. Shechtman, F. Durand, W. T. Freeman, and T. Park. One-step diffusion with distribution matching distillation. In *Proceedings of the IEEE/CVF conference on computer vision and pattern recognition*, pages 6613–6623, 2024.
- [76] B. J. Zhang, T. Sahai, and Y. M. Marzouk. A koopman framework for rare event simulation in stochastic differential equations. *Journal of Computational Physics*, 456:111025, 2022.
- [77] R. Zhang, P. Isola, A. A. Efros, E. Shechtman, and O. Wang. The unreasonable effectiveness of deep features as a perceptual metric. In *Proceedings of the IEEE conference on computer vision and pattern recognition*, pages 586–595, 2018.
- [78] Y. Zhang, C. Deck, A. Tagliasacchi, J. Sohl-Dickstein, P. Jaini, and T. Zhang. Fast training of diffusion models via operator learning. In *International Conference on Learning Representations (ICLR)*, 2023.
- [79] H. Zheng, W. Nie, A. Vahdat, K. Azizzadenesheli, and A. Anandkumar. Fast sampling of diffusion models via operator learning. In *International conference on machine learning*, pages 42390–42402. PMLR, 2023.
- [80] L. Zhou, A. Lou, S. Khanna, and S. Ermon. Denoising diffusion bridge models. *arXiv preprint arXiv:2309.16948*, 2023.

- [81] M. Zhou, H. Zheng, Z. Wang, M. Yin, and H. Huang. Score identity distillation: Exponentially fast distillation of pretrained diffusion models for one-step generation. In *Forty-first International Conference on Machine Learning*, 2024.
- [82] Z. Zhou, D. Chen, C. Wang, C. Chen, and S. Lyu. Simple and fast distillation of diffusion models. *Advances in Neural Information Processing Systems*, 37:40831–40860, 2024.

A Proof of Theorem 5.1

For the reader’s convenience, we restate the theorem.

Theorem (Finite Koopman Approximation for Analytic Dynamics). *Let $\Phi : \mathbb{R}^n \rightarrow \mathbb{R}^n$ be an analytic map, and let $x_T \sim \mathcal{N}(0, I_n)$. Then, for any $\epsilon > 0$, there exists a linear operator $C \in \mathbb{R}^{d \times d}$ such that*

$$\mathbb{E} [\|\xi(\Phi(x_T)) - C\xi(x_T)\|^2] \leq \epsilon ,$$

where $\xi : \mathbb{R}^n \rightarrow \mathbb{R}^d$ denotes the observable lifting map. Moreover, the required dimension d grows at most polynomially with $1/\epsilon$, and the mapping Φ can be approximated arbitrarily well using multivariate polynomials up to degree d .

Proof. Since $\Phi : \mathbb{R}^n \rightarrow \mathbb{R}^n$ is analytic, for every $\delta > 0$ and every compact set $K \subset \mathbb{R}^n$, there exists a multivariate polynomial map $p : \mathbb{R}^n \rightarrow \mathbb{R}^n$ such that

$$\sup_{x \in K} \|\Phi(x) - p(x)\| \leq \delta ,$$

which follows from the theory of approximation by Taylor polynomials for analytic functions [71].

Let $x_T \sim \mathcal{N}(0, I_n)$. Since x_T has exponentially decaying tails [72], for any $\eta > 0$ there exists $R > 0$ such that

$$\mathbb{P}(x_T \notin B_R) \leq \eta ,$$

where $B_R = \{x \in \mathbb{R}^n : \|x\| \leq R\}$. Restricting attention to B_R , we consider the polynomial approximation p of Φ with error at most δ .

Now, following the result of Iacob et al. [26], for the polynomial map p , there exists a finite-dimensional lifting map $\xi : \mathbb{R}^n \rightarrow \mathbb{R}^d$ consisting of monomials up to some degree, and a linear operator $C \in \mathbb{R}^{d \times d}$, such that

$$\xi(p(x)) = C\xi(x)$$

for all $x \in \mathbb{R}^n$. In particular, on B_R ,

$$\|\xi(\Phi(x)) - C\xi(x)\| \leq \|\xi(\Phi(x)) - \xi(p(x))\| ,$$

since $\xi(p(x)) = C\xi(x)$ exactly.

Since ξ is a smooth (polynomial) map, there exists a Lipschitz constant $L > 0$ depending on the derivatives of ξ over B_R , such that

$$\|\xi(\Phi(x)) - \xi(p(x))\| \leq L\|\Phi(x) - p(x)\| \leq L\delta$$

for all $x \in B_R$.

Thus, for $x_T \in B_R$,

$$\|\xi(\Phi(x_T)) - C\xi(x_T)\| \leq L\delta .$$

Outside B_R , the trivial bound

$$\|\xi(\Phi(x_T)) - C\xi(x_T)\| \leq 2M$$

holds for some finite constant $M > 0$, due to the polynomial growth of ξ and the Gaussian decay of x_T .

Hence, the expected Koopman error satisfies

$$\mathbb{E} [\|\xi(\Phi(x_T)) - C\xi(x_T)\|^2] \leq (1 - \eta)L^2\delta^2 + \eta(2M)^2 .$$

Given any $\epsilon > 0$, we can choose η sufficiently small so that $\eta(2M)^2 \leq \epsilon/2$, and then δ sufficiently small so that $(1 - \eta)L^2\delta^2 \leq \epsilon/2$.

Notably, the degree of the polynomial map p needed, and hence the number of monomials d in ξ , grows at most polynomially with $1/\delta$ and thus with $1/\epsilon$, concluding the proof.

We further note that the function Φ implemented by DhariwalUNet [28] is analytic. Specifically, each module composing the network—including convolutions, SiLU activations, residual connections, attention mechanisms, and group normalization with $\epsilon > 0$ —is an analytic function. Since compositions of analytic functions remain analytic, it follows that the entire forward pass Φ is analytic on \mathbb{R}^n .

□

B Proof of Theorem 5.2

We restate the theorem for the readers' convenience.

Theorem (Semantic Proximity via Koopman-Invariant Coordinates). *Let $\Phi_t : \mathbb{R}^n \rightarrow \mathbb{R}^n$ be the reverse diffusion flow of a trained model (from time T to 0), and let $\mathcal{O} \subset L^2(\mathbb{R}^n)$ be a finite-dimensional subspace such that:*

1. $\mathcal{K}_t \mathcal{O} \subset \mathcal{O}$ for all $t \in [0, T]$,
2. $\exists C_t : \mathbb{R}^d \rightarrow \mathbb{R}^d$ such that $\mathcal{K}_t \xi = \xi \circ \Phi_t = C_t \xi$ for all $\xi \in \mathcal{O}$,
3. Φ_T is locally Lipschitz.

For any $x_T^1, x_T^2 \in \mathbb{R}^n$, define $x_0^j := \Phi_T(x_T^j)$ for $j = 1, 2$, and let $\xi : \mathbb{R}^n \rightarrow \mathbb{R}^d$ be the vector-valued observable $\xi(x) := (\xi_1(x), \dots, \xi_d(x)) \in \mathcal{O}$. Then:

$$\|x_0^1 - x_0^2\| \leq L \cdot \|\Phi_T(x_T^1) - \Phi_T(x_T^2)\| \leq L \cdot \|C_T\| \cdot \|\xi(x_T^1) - \xi(x_T^2)\|.$$

Proof. Let $\Phi_t : \mathbb{R}^n \rightarrow \mathbb{R}^n$ denote the reverse diffusion dynamics. Based on the proof of Thm. 5.1, there exists a linear operator $C_t : \mathbb{R}^d \rightarrow \mathbb{R}^d$ satisfying

$$\mathcal{K}_t \xi = \xi \circ \Phi_t = C_t \xi,$$

for every $\xi \in \mathcal{O}$ and $t \in [0, T]$.

Define the vector-valued map for the basis $\{\xi_j\}$ of \mathcal{O}

$$\xi(x) := (\xi_1(x), \dots, \xi_d(x)) \in \mathbb{R}^d.$$

Since the ξ_j are smooth and capture independent semantic directions, ξ is locally bi-Lipschitz near typical x_T . That is, there exist constants $C_1, C_2 > 0$ such that

$$C_1 \|\xi(x_T^1) - \xi(x_T^2)\| \leq \|x_T^1 - x_T^2\| \leq C_2 \|\xi(x_T^1) - \xi(x_T^2)\|.$$

Because Φ_T is locally Lipschitz, there exists $L > 0$ such that

$$\|\Phi_T(x_T^1) - \Phi_T(x_T^2)\| \leq L \|x_T^1 - x_T^2\|.$$

Substituting the bi-Lipschitz inequality yields

$$\|\Phi_T(x_T^1) - \Phi_T(x_T^2)\| \leq LC_2 \|\xi(x_T^1) - \xi(x_T^2)\|.$$

Moreover, by Koopman linearity,

$$\xi(\Phi_T(x_T^j)) = C_T \xi(x_T^j), \quad j = 1, 2,$$

and therefore

$$\xi(\Phi_T(x_T^1)) - \xi(\Phi_T(x_T^2)) = C_T (\xi(x_T^1) - \xi(x_T^2)).$$

Thus, proximity in $\xi(x_T)$ coordinates implies proximity of final samples x_0^1 and x_0^2 under Φ_T . □

C Factorized Koopman Matrix for Fast Eigenspectrum penalty

To enable control over eigenvalues of the Koopman operator, we describe an efficient implementation of our Koopman-based Distillation Method (KDM), which we term KDM-F, alleviating the need for computation of the eigendecomposition during training. Since every matrix $C := C_\eta$ is diagonalizable up to an arbitrarily small perturbation of the entries [2], we can write:

$$C = P\Lambda P^{-1}$$

where $P \in \mathbb{C}^{d \times d}$ is an invertible matrix and $\Lambda = \text{diag}(\lambda_1, \dots, \lambda_d) \in \mathbb{C}^{d \times d}$. This way enables efficient implementation of spectral penalties on Λ , without the need to compute it on the fly during training.

To represent this decomposition within a real-valued neural network framework, we learn the real and imaginary components of the Koopman eigenvectors separately. Specifically, two orthonormal matrices, P_{re} and P_{im} , represent the real and imaginary parts of the eigenvectors. These are combined into a real-valued block matrix using the standard transformation for complex-to-real matrix representation:

$$P = \begin{bmatrix} P_{\text{re}} & -P_{\text{im}} \\ P_{\text{im}} & P_{\text{re}} \end{bmatrix} \in \mathbb{R}^{2d \times 2d}.$$

Rather than explicitly computing the inverse P^{-1} , we parameterize a separate learnable matrix P_{inv} with the same structure, constructed analogously from two unconstrained real matrices. This improves flexibility and avoids numerical instability associated with matrix inversion.

The eigenvalues of the Koopman operator are encoded using polar coordinates. Specifically, the modulus and phase of each eigenvalue are parameterized as

$$\lambda_j = e^{-\exp(\nu_j)} \cdot e^{i\theta_j} = e^{-\exp(\nu_j)} (\cos(\theta_j) + i \sin(\theta_j)),$$

where ν_j and θ_j are learnable parameters. Let $\lambda_{\text{re}} = (\text{real}(\lambda_j))$, $\lambda_{\text{im}} = (\text{imag}(\lambda_j)) \in \mathbb{R}^d$ be the aggregated vector of real and imaginary parts of the eigenvalues, respectively. We assemble these values into a real-valued block-diagonal matrix:

$$\Lambda = \begin{bmatrix} \text{diag}(\lambda_{\text{re}}) & -\text{diag}(\lambda_{\text{im}}) \\ \text{diag}(\lambda_{\text{im}}) & \text{diag}(\lambda_{\text{re}}) \end{bmatrix} \in \mathbb{R}^{2d \times 2d}.$$

At inference time, the latent state vector $z \in \mathbb{R}^d$ is first augmented to \mathbb{R}^{2d} by concatenating a zero vector: $\tilde{z} = [z; 0]$. The evolution under the Koopman operator is then computed as

$$z_{\text{next}} = P_{\text{inv}} \Lambda P \tilde{z}.$$

Finally, we discard the imaginary part and retain only the first d entries to return a real-valued output of the same dimensionality as the input.

This formulation enables us to simulate rich, expressive dynamics through a fully linear evolution in the lifted Koopman space, while maintaining computational tractability and interpretability. Moreover, this decomposition is particularly amenable to distillation: the structure of the transformation ensures that semantic and temporal coherence is preserved during student training, as the model explicitly disentangles dynamics into magnitude and phase components.

D Additional Experiments and Analysis

D.1 Ablation Studies

Loss Ablation Study. We conduct an ablation study to evaluate the contribution of each loss component. As shown in Tab. 5, using only $\mathcal{L}_{\text{pred}}$ or any pairwise combination of the Koopman-related losses still enables the model to learn, as indicated by moderate FID and IS scores. However, incorporating all three losses together, including $\mathcal{L}_{\text{Koopman}}$, creates a synergistic effect—reducing the FID from around 10 to 7.83 and achieving a higher IS than any partial combination. Finally, we highlight the importance of incorporating an adversarial setup, which further improves both FID and IS scores by enhancing perceptual quality.

Table 5: Koopman losses ablation; bold is best and underscore is second-best.

	\mathcal{L}_{lat}	$\mathcal{L}_{\text{pred}}$	\mathcal{L}_{rec}	$\mathcal{L}_{\text{lat}} + \mathcal{L}_{\text{pred}}$	$\mathcal{L}_{\text{rec}} + \mathcal{L}_{\text{pred}}$	$\mathcal{L}_{\text{rec}} + \mathcal{L}_{\text{lat}}$	$\mathcal{L}_{\text{Koopman}}$	\mathcal{L}
FID	487	11.2	457	9.53	10.7	11.16	<u>7.83</u>	4.97
IS	1.00	8.23	1.00	8.82	8.26	8.68	<u>8.83</u>	9.22

Empirical Investigation of Koopman Matrix Size. We evaluate the impact of varying the size of the Koopman matrix. As shown in Tab. 6, smaller matrices tend to generalize better than larger ones. This result is somewhat counterintuitive, as the scaling experiments in Sec. 6.2 demonstrate a clear trend where increasing the number of parameters typically improves performance. We hypothesize that smaller matrices generalize more effectively, and we leave a deeper understanding of this phenomenon—through the lens of dynamical systems theory and empirical analysis—for future research.

Table 6: FID scores across matrix sizes on the CIFAR-10 unconditional task; bold is best.

Size	1024	4096	9216
FID	5.08	7.24	9.41

D.2 Additional Qualitative Results

We include additional qualitative results of our method, extending the evaluation presented in the main text on more datasets and testing scenarios.

Additional Comparison of Student vs Teacher. In Figs. 6, 7, 8, and 9, we present generations from our model alongside those of the original EDM model. Corresponding blocks indicate samples generated from the same initial noise.



Figure 6: Unconditional Generation of FFHQ. Sampled images using 79 NFEs with EDM [28] (left), and using 1 NFE with KDM (right).



Figure 7: Unconditional Generation of FFHQ. Sampled images using 79 NFEs with EDM [28] (left), and using 1 NFE with KDM (right).

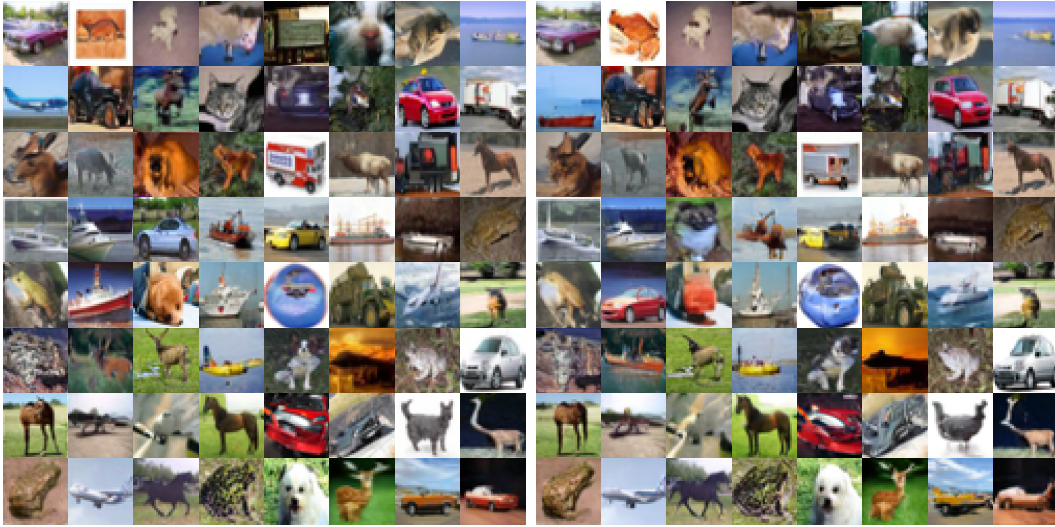


Figure 8: Unconditional Generation of CIFAR-10. Sampled images using 35 NFEs with EDM [28] (left), and using 1 NFE with KDM (right).

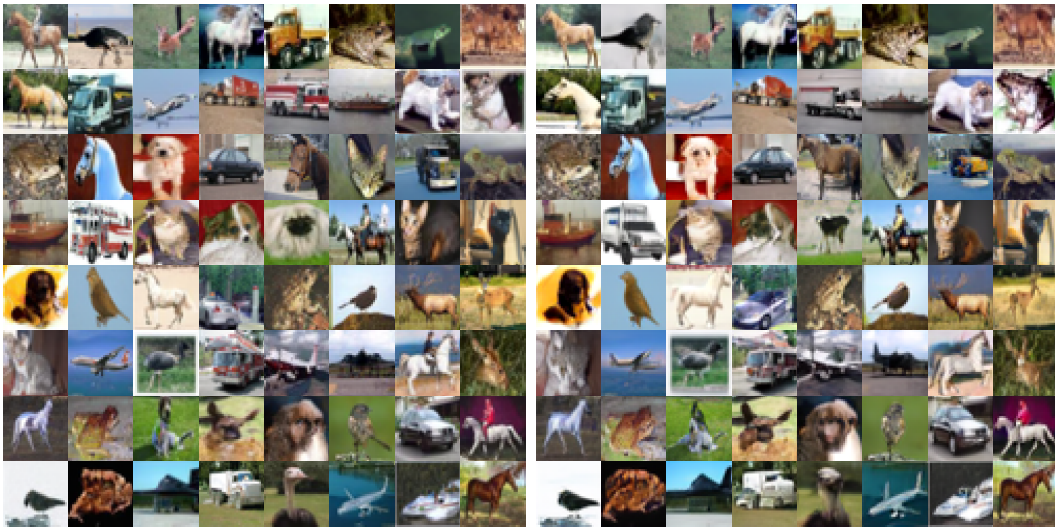


Figure 9: Conditional Generation of CIFAR-10. Sampled images using 35 NFEs with EDM [28] (left), and using 1 NFE with KDM (right).

Additional Local Structure Analysis. We extend the experiment from Sec. 6.1 to AFHQv2, conditional CIFAR-10, and unconditional CIFAR-10 datasets, as shown in Fig. 10, Fig. 11, and Fig. 12, respectively. The results reinforce the conclusions of the main experiment: both EDM and our distilled model exhibit local semantic coherence, preserving features such as position, color, identity, and more—even when traversing farther from the original point in noise space.

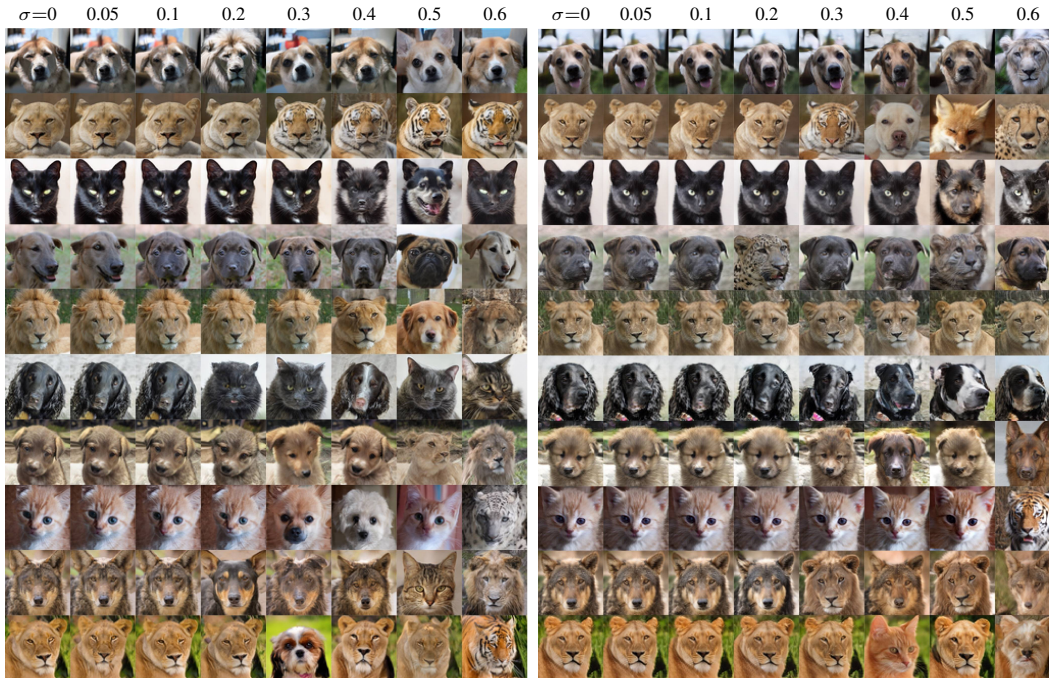


Figure 10: Unconditional AFHQv2: Comparison of neighborhood exploration across different noise levels σ . Left: EDM [28]. Right: our method. Each image corresponds to a small perturbation around the original noise sample.

D.3 Running GET Method with GANs

Throughout our work, we made a concerted effort to compare our method against GET using their publicly available implementation. In particular, we aimed to evaluate the effect of adding adversarial loss to their framework, as we do in our own ablation studies. Unfortunately, we encountered two major obstacles. First, as shown in Sec. 4, the GET method is extremely computationally intensive—nearly four times slower than our approach. This makes it impractical to run full experiments on our infrastructure. For example, training our method on a single A6000 GPU requires approximately 120 hours, while training GET under similar conditions takes around 480 hours, exceeding our available computational resources. Second, despite these challenges, we attempted to integrate the adversarial loss into GET’s pipeline. However, the resulting model proved unstable, often collapsing during training. Due to these combined computational and methodological limitations, we were unable to complete a controlled comparison under the same extended conditions. We hope future work will revisit this question under more favorable resource constraints.

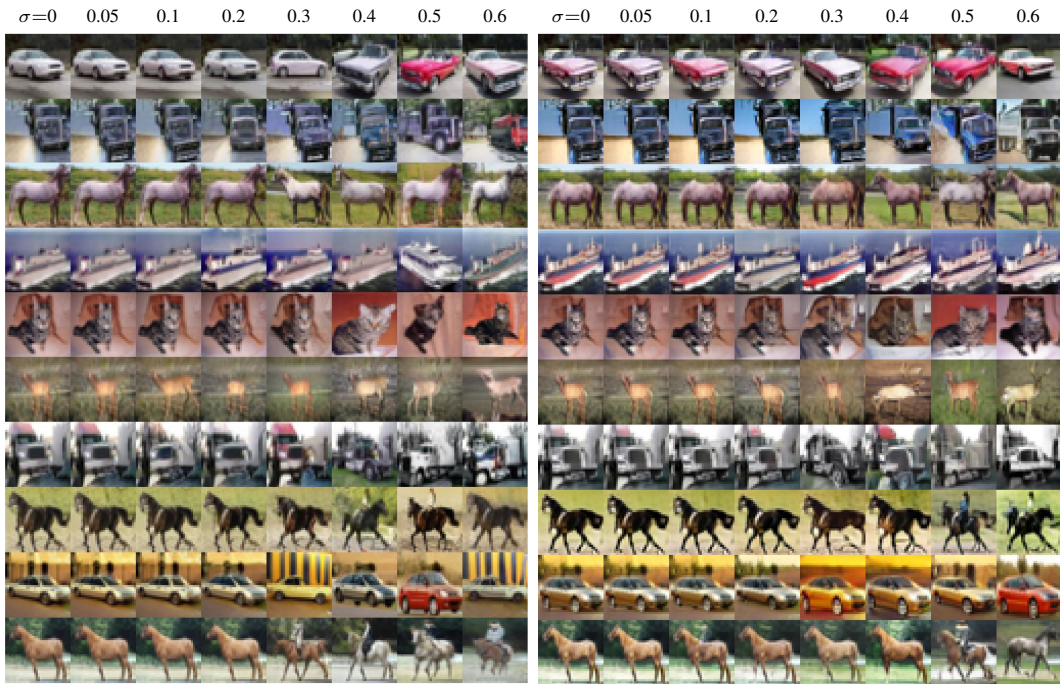


Figure 11: Conditional CIFAR-10: Comparison of neighborhood exploration across different noise levels σ . Left: EDM [28]. Right: our method. Each image corresponds to a small perturbation around the original noise sample.

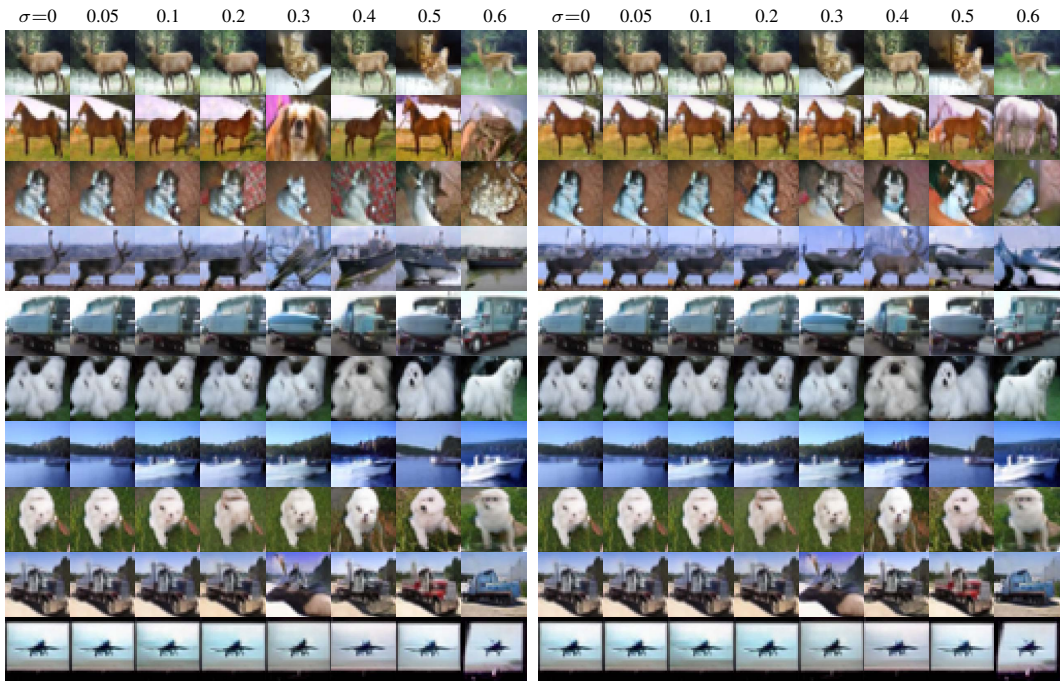


Figure 12: Unconditional CIFAR-10: Comparison of neighborhood exploration across different noise levels σ . Left: EDM [28]. Right: our method. Each image corresponds to a small perturbation around the original noise sample.

E Additional Details

E.1 Training and Sampling Procedures Pseudo-codes

The training process of the model follows a Koopman-inspired backward mapping approach, augmented with adversarial supervision. Given a clean-noisy pair (x_0, x_T) , the model learns a latent Koopman operator that evolves the noisy encoding backward to approximate the clean encoding, while a decoder reconstructs the input from the latent space. The model also supports class-conditional dynamics via Koopman control.

Algorithm 1 Training Procedure

Require: Training pairs (x_0, x_T) , labels y (optional), model $E_\phi, E_\psi, C_\eta, D_\psi$ discriminator D_γ

- 1: **for** each training step **do**
 - 2: Encode $z_0 \leftarrow E_\phi(x_0, 0, y)$
 - 3: Encode $z_T \leftarrow E_\psi(x_T, T, y)$
 - 4: Add noise: $\tilde{z}_0 \leftarrow z_0 + \epsilon_0, \tilde{z}_T \leftarrow z_T + \epsilon_T$, where $\epsilon_T, \epsilon_0 \sim \mathcal{N}(0, 0.4)$
 - 5: Push via Koopman: $z_0^{\text{push}} \leftarrow C_\eta(\tilde{z}_T)$
 - 6: **if** conditional Koopman **then**
 - 7: Add control: $z_0^{\text{push}} \leftarrow z_0^{\text{push}} + C_\mu(y)$
 - 8: **end if**
 - 9: Decode: $\hat{x}_0 \leftarrow D_\psi(\tilde{z}_0, 0, y)$
 - 10: Decode pushed: $\hat{x}_0^{\text{push}} \leftarrow D_\psi(z_0^{\text{push}}, 0, y)$
 - 11: Compute latent loss: $\mathcal{L}_{\text{lat}} \leftarrow \|z_0 - z_0^{\text{push}}\|^2$
 - 12: Compute reconstruction loss: $\mathcal{L}_{\text{rec}} \leftarrow d(x_0, \hat{x}_0)$
 - 13: Compute full pass loss: $\mathcal{L}_{\text{pred}} \leftarrow d(x_0, \hat{x}_0^{\text{push}})$
 - 14: Compute model adversarial loss: $\mathcal{L}_{\text{adv}}^G \leftarrow CE(1, D_\gamma(\hat{x}_0^{\text{push}}))$
 - 15: Compute discriminator loss: $\mathcal{L}_{\text{adv}}^D \leftarrow CE(1, D_\gamma(x_0)) + CE(0, D_\gamma(\hat{x}_0^{\text{push}}))$
 - 16: model Combine losses:

$$\mathcal{L}_{\text{total}} \leftarrow \mathcal{L}_{\text{rec}} + \mathcal{L}_{\text{pred}} + \mathcal{L}_{\text{lat}} + w_{\text{adv}} \cdot \mathcal{L}_{\text{adv}}^G$$
 - 17: Update $E_\phi, E_\psi, C_\eta, C_\mu, D_\psi$ and D_γ via backpropagation
 - 18: **end for**
-

d is a distance measure such as MSE or LPIPS. We utilize LPIPS. CE is cross-entropy loss. At inference time, the model can sample clean images by reversing from random Gaussian noise x_T , applying the Koopman operator in latent space, and decoding to the image space.

Algorithm 2 Sampling Procedure

Require: Koopman model: $E_\phi, C_\eta, C_\mu, D_\psi$, labels y (optional)

- 1: Sample noise $x_T \sim \mathcal{N}(0, \sigma^2)$
 - 2: Encode: $z_T \leftarrow E_\psi(x_T, T, y)$
 - 3: Push: $z_0^{\text{push}} \leftarrow C_\eta(z_T)$
 - 4: **if** conditional Koopman **then**
 - 5: Add control: $z_0^{\text{push}} \leftarrow z_0^{\text{push}} + C_\mu(y)$
 - 6: **end if**
 - 7: Decode: $\hat{x}_0 \leftarrow D_\psi(z_0^{\text{push}}, 0, y)$
 - 8: **return** Clean sample \hat{x}_0
-

E.2 Datasets Collection

For the **Checkerboard** dataset, we sampled using 10 NFEs with EDM [28] or flow matching [40]. Following [19], we sampled **CIFAR-10** with 35 NFEs from EDM. For **FFHQ** and **AFHQv2**, we used 79 NFEs using EDM, as recommended.

E.3 Method Implementation Details

We provide the full code implementation for the Checkerboard and CIFAR-10 (both conditional and unconditional) datasets in the supplementary material. Due to memory constraints, the implementations for FFHQ and AFHQv2 will be released shortly. In this section, we briefly describe the implementation details of each method, while we encourage the reader to refer to the codebase for exact configurations. We train our models for 800k iterations with the Adam optimizer [33] at a fixed learning rate of $3e-4$. We do not use warm-up, weight decay, or any learning-rate schedule.

Checkerboard. For this dataset, we build upon the implementation of [41]. Both x_0 and x_T are encoded using the same denoising architecture as described in their work. The decoding of z_0 is performed using the inverse of this module. The Koopman operator is implemented as a simple linear layer. Complete implementation details are available in the shared code.

CIFAR-10, FFHQ, and AFHQv2. We adopt the SongUNet architecture from [28] for encoding x_0 and x_T , as well as for decoding z_0 . To reduce latent dimensionality, the output channels of the network are set to 1, effectively reducing the latent space size by a factor of 3. The Koopman operator is implemented either as a standard linear transformation or using our custom Fast Koopman module. To maintain architectural fairness, we downscale all networks to match the total parameter count of the original Karras network [28] and the GET distillation model [19]. The FFHQ and AFHQv2 configurations follow a similar encoder-decoder structure with one key difference: a linear projection layer is appended to the end of the encoder and the beginning of the decoder to further control the latent space dimensionality. All other aspects remain consistent across datasets. Note that the discriminator is trained using a separate optimizer, akin to the Koopman module’s optimizer.

Hyperparameters and Training. We provide complete training scripts along with plug-and-play configuration files in the supplementary material. An overview of the key hyperparameters used for each dataset is summarized in Tab. 7. Overall, our method requires minimal hyperparameter tuning and we did not perform any hyperparameter search.

- **Unet Out Channels:** Controls the number of output channels in SongUNet.
- **Unet Model Channels:** Determines the internal channel width, affecting the model’s capacity.
- **Noisy Latent Injection:** A Gaussian noise term $\epsilon \sim \mathcal{N}(0, 1)$ added to latents (as described in the pseudocode) to improve generalization and mitigate numerical instabilities.
- **Adversarial Weight:** Applied to the adversarial loss term in our generator loss; not used for the discriminator loss directly.
- **Linear Module:** Indicates the presence of an additional linear layer for compressing the latent space, applied at the output of the encoder and the input of the decoder.

Table 7: Model Hyperparameters Across Datasets

Configuration	Checkerboard	CIFAR-10	FFHQ	AFHQv2
Batch Size	4096	128	64	64
Learning Rate (LR)	0.0003	0.0003	0.0003	0.0003
Iterations	800k	800k	800k	800k
Unet Out Channels	1	1	1	1
Unet Model Channels	64	64	32	32
Noisy Latent Injection	0.4	0.4	0.4	0.4
Adversarial Weight	0.01	0.01	0.01	0.01
Linear Module	No	No	Yes	Yes
Latent Dim Size	1024	1024	512	512

E.4 Human Evaluation Experiment

While the Fréchet Inception Distance (FID) is widely used to evaluate the quality of images generated by generative models, recent studies have highlighted its limitations in aligning with human judgments

Table 8: Human Evaluation of Image Realism. The reported ratio reflects the number of times participants selected the model-generated collage as more realistic, out of a total of 300 evaluations.

	EDM (Teacher)	KDM (Student)
Ratio	45%	55%

of image realism. For instance, Jayasumana et al. [27] demonstrate that FID can contradict human evaluations, particularly in assessing perceptual quality and semantic alignment, due to its reliance on Inception-v3 features and the assumption of Gaussian distributions. Similarly, Otani et al. [54] emphasize that automatic metrics like FID often fail to capture the nuanced aspects of human perception, underscoring the need for standardized human evaluation protocols. Furthermore, Kynkäänniemi et al. [38] reveal that FID can be manipulated by aligning top-N class histograms without genuinely improving image quality, indicating potential biases in the metric. These findings suggest that while FID provides a useful quantitative signal, it may not fully encapsulate human perceptions of image realism, highlighting the importance of incorporating human evaluations when assessing generative models.

Therefore, in the main paper, we report the results of a human evaluation experiment designed to compare our method against EDM. Specifically, we curated 10 image collages (6×6) of human faces generated by the teacher model (EDM, 79 NFEs) and 10 collages generated by our student model (1 NFE), using samples from the FFHQ dataset. Each comparison slide presents one collage from each model, displayed side-by-side as illustrated in Fig. 4, with the order randomized. We then asked 30 human raters to evaluate 10 such slides and choose, for each, which collage appeared more realistic. If both appeared equally realistic, they were instructed to make a random choice. This process yielded 300 total decisions. We report in the main paper and in Tab. 8, the proportion of times each model was preferred. Finally, we attach to the appendix both the slides that we sent to the practitioners and the Excel that aggregates the results. The results indicate that decisions were made almost at random, suggesting that participants had difficulty distinguishing between the student and teacher generations. This implies that, despite existing FID gaps, human evaluators found it hard to perceive meaningful differences. Participants reported that both collages included highly realistic images, as well as images with noticeable artifacts that appeared unrealistic, in their judgment.

E.5 Parameter Scaling

We report the full results of the scaling experiment shown in Sec . 6.2, including IS score from the parameter scaling comparison in Tab. 9. The results demonstrate that our approach consistently outperforms GET in terms of FID across all model sizes, except for IS in 20M, indicating superior perceptual quality. Notably, the improvement is more pronounced as the model size increases, with our 84M model achieving an FID of 4.89 compared to 7.19 for GET. In terms of IS, our method matches or surpasses GET, with particularly strong results at larger scales. These results underscore the scalability and effectiveness of our approach.

Table 9: FID and IS scores for different model sizes, comparing our approach with GET.

	20M		38M		84M	
	Ours	GET	Ours	GET	Ours	GET
FID	10.2	10.72	5.04	8.00	4.89	7.19
IS	8.50	8.69	9.12	9.03	9.11	9.09

E.6 Extended Outlier Analysis

In Sec. 6.1, we present the results of our model’s component (left side) in the experiment shown in Fig. 13. Outlier detection was performed using the DBSCAN algorithm with a distance threshold of 0.15. Interestingly, our model exhibits a slightly increased number of outliers. We hypothesize that this may be due to early stopping during training, as our primary objective was not to maximize performance on this particular dataset, but rather to gain insight and intuition into the nature of the learned dynamics. Finally, we observe that the outlier phenomenon is inherited from the teacher model (right side), suggesting that it is a more general characteristic of the generative dynamics rather than an artifact introduced by the distillation process.

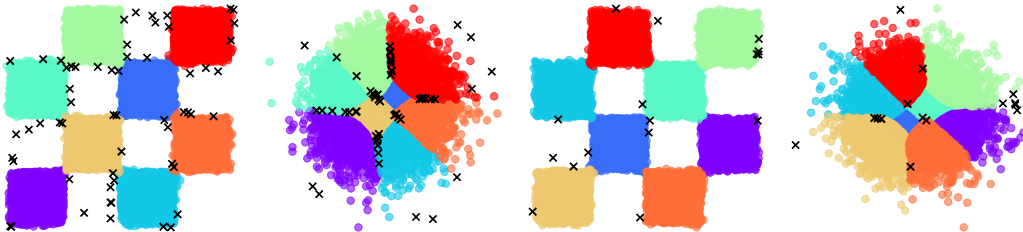


Figure 13: Outlier analysis on generated checkerboard patterns. The two left images are our model (student), and the two images on the right are from the flow matching model (teacher).

F Additional Discussion of Future Work and Current Limitations

In this study, we took a significant step toward leveraging dynamical systems theory for offline distillation, demonstrating its strong potential in this domain. In this section, we outline several future research directions that we believe are both promising and intellectually compelling.

Standalone Koopman Generative Model. Koopman theory enables modeling nonlinear dynamical systems in a transformed space where they can be analyzed linearly. This raises an intriguing question: *Can the Koopman framework serve as a standalone generative model, capable of learning data distributions from scratch?* While the question remains open, exploring this direction could yield a novel and theoretically grounded framework for generative modeling.

Utilization of Full Trajectory Information. Our current offline setup relies solely on noise-data pairs extracted from pre-trained teacher models. However, the diffusion process inherently includes intermediate steps that are discarded. We hypothesize that leveraging this full trajectory information could enhance trajectory alignment and improve student performance. Moreover, Koopman theory naturally accommodates multi-step signals, making this a promising direction for further investigation. Additionally, the current framework does not support a quality-versus-sampling-steps trade-off, which some online methods do enable. Future work incorporating the full diffusion trajectory could integrate this flexibility into our approach.

Incorporating Broader Koopman Theory Literature. The connection between Koopman theory and diffusion model distillation opens the door to a rich body of theoretical and practical tools. On the theoretical side, works on sample complexity and error bounds for Koopman operators [56, 10, 51] may provide insights into convergence guarantees. Information-theoretic perspectives [42] could offer new modeling constraints or regularization schemes. On the practical side, methods for rare-event sampling [76] may improve long-tail generation capabilities. Finally, while the current mathematical formulation supports discrete Koopman evaluation, the underlying theory naturally extends to continuous settings as well. Exploring these directions could substantially extend and generalize the impact of our framework.

Enhancing the Adversarial Setup. While adversarial components have been shown to be critical in many distillation methods [74, 32], our current implementation uses a basic discriminator architecture with standard loss functions and training schemes. We believe that integrating more advanced

adversarial paradigms could significantly boost performance, potentially closing the gap with state-of-the-art online distillation methods.

Decision Boundary Insights. In our synthetic experiments, we identified a common cause underlying failure modes or “outliers” in the generative dynamics. Further investigation is needed to determine whether this phenomenon generalizes to more complex datasets. If it does, it could guide the development of strategies such as uncertainty estimation, selective sampling to avoid generating low-quality outputs, incorporating structural constraints into the latent space to prevent such failures, or introducing auxiliary self-supervised objectives—such as contrastive learning—to enhance the model’s ability to distinguish between semantically similar groups.

Toward Broader Applications. Due to limited computational resources, we were unable to extend our offline distillation framework to more complex tasks, such as text-to-image generation, that require large-scale compute infrastructures. It will be interesting to explore how our method can scale or adapt to other domains and tasks. Additionally, because our method makes no assumptions about the initial and terminal states of the underlying dynamical system, we believe it is applicable to a broader class of generative models, including DDBMs [80], stochastic interpolants [1], and others [13].